Chapter 4

Estimation of the topological charge of the helical beam from the random light

In this chapter, we discuss a non-interferometric technique to estimate the OAM of the helical beam by counting the number of petals from the scrambled light. A detailed theoretical basis, numerical simulation, and experimental results are explained.

4.1 Introduction

The light signal carries orbital angular momentum (OAM) of $l\hbar$ per photon associated with their helical wavefronts and exhibits great potential for practical applications (Allen, 1992; Torres, 2011). For instance, significant applications are particle trapping (Shi, 2019), free-space optical communication (Willner, 2015), etc. On the other hand, the topological charge (TC) or OAM has been applied to create an infinite-dimensional discrete basis to increase the transmitting capacity of the encoded information in optical quantum communication (Willner, 2015). The OAM mode of the light is a significant parameter for fundamental and practical reasons. Therefore, determining the OAM associated with a beam becomes significant. In principle, estimation of the OAM mode requires evaluation of the helical wavefront of the light, and several techniques have been proposed for this purpose. Some of these methods are based on interference (Ghai, 2008; Khajavi, 2018; Leach, 2004; Sztul, 2006; Zhao, 2020) and diffraction (Araujo, 2011; Ferreira, 2011; Li, 2020; Melo, 2018; Princeton, 2019; Singh, R., 2007; Zheng, 2017). In a recent development, a gradually changing-period spiral spoke grating (GCPSSG) was introduced to monitor the magnitude and sign of the TC of the helical beam. The magnitude of TC was evaluated by enumerating the petal in the diffraction pattern and the sign was distinguished from the rotation of the twisted fringes with respect to the grating (Li, 2020). However, these techniques are mainly limited to the propagation of the vortex beams through homogenous media or free space.

On the other hand, propagation of a beam through random media affects the properties such as beam shape, coherence, etc, and consequently determinantal on the performance of the beam in several practical applications (Gbur, 2008). When the vortex beam is transmitted through random media such as atmospheric turbulence, or underwater

for optical communication then scattering is a common phenomenon there and the helical wavefront of the vortex beam gets scrambled. The complex spatial structure of the scrambled optical field is referred to as the speckle field. The scrambled light from random scattering media plays a crucial role in optical quantum communication, imaging, and remote sensing (Gong, 2019; Malik, 2012; Chen, L., 2014). The scattering media scrambles the incident wavefront due to the inhomogeneity in the optical path lengths of the scattering media and creates a speckle pattern. Therefore, direct detection of the incident wavefront directly from the speckle pattern is a difficult task with the previously proposed techniques (Araujo, 2011; Ferreira, 2011; Ghai, 2008; Khajavi, 2018; Li, 2020; Leach, 2004; Melo, 2018; Princeton, 2019; Singh, R., 2007; Sztul, 2006; Zheng, 2017; Zhao, 2020). Researchers have proposed wavefront correction techniques to recover the wavefront from the scrambled light. These techniques were based on optical transmission matrix, time reversal, and phase conjugation (Hillman, 2013; Park, 2017; Popoff, 2010). The wave equations are symmetric with respect to forward and backward traveling waves. By adopting this analogy the back surface of the object was illuminated with the time reverse field and then backpropagated the field in the scattering object at the object's front face after transmission through the scattering media to recover the initial wavefront. In a recent development, the holographic set-up with the Hanbury-Brown Twiss (HBT) approach for polarized light was used to measure generalized SPs and also detect the helical phase structure from the speckle pattern (Vinu, 2015, 2016). A distribution of cross-covariance of the random intensity pattern was utilized to estimate the TC by enumerating the number of petals (Chen, 2021). In addition, some significant detection techniques have been developed in the last decade to detect the TC and spiral phase profile of the helical beam with partially coherent light (Ding, 2014; Lu, 2019; Singh, R., 2015). Recently, incoherent light has also been explored to develop detection schemes for

the recovery of TC and spiral phase profile of the helical beam propagating through rough scattering layers (Bezerra, 2020; Huang, 2021; Liu, 2019).

In this Chapter, we propose a new approach to estimate the TC of the incident helical beam from the random light using higher-order Stokes parameters (SPs) correlation. Here we present a new theoretical basis to estimate the TC of the incident helical beam propagating through the scatterer by applying higher-order SPs correlation. To develop a new theoretical basis, SPs of the random light is used and higher-order correlations between SPs fluctuations are evaluated. This provides a 4x4 correlation matrix that contains 16 elements. Out of these 16 elements only one element is considered to build a theoretical basis and subsequently apply for the estimation of the TC of the incident helical beam. To validate the proposed approach, we designed a highly stable experimental geometry in a coaxial propagation of two orthogonal polarization states of the light and use this configuration to estimate the TC of the incident helical beam from the random light. A detailed theoretical model, numerical simulation, and experimental results are presented below.

4.2 Theoretical basis

Let us consider an orthogonally polarized monochromatic light source. The x-polarization state of the beam is loaded with a spiral wavefront and the y-polarization state is a plane wave. These two orthogonal polarization states coaxially travel along the z-direction. The complex amplitude at the z=0 plane is expressed as

$$E(\hat{r}) = A_m(\hat{r})\exp(il\varphi)\hat{e}_x + A_0(\hat{r})\hat{e}_y, \tag{4.1}$$

where $\hat{e}_x$ and $\hat{e}_y$ represent the x and y polarization states of the light respectively and $\hat{r}$ is the position vector at the transverse plane. $A_l(\hat{r})$, $A_0(\hat{r})$ indicate the real-valued amplitude

of the helical beam and plane wave. The term $\exp(il\varphi)$ denotes the helical wavefront with the TC *l* of the helical beam and $\varphi = \tan^{-1}\left(\frac{y}{x}\right)$, is the azimuthal angle.

Now the beam propagates through a random scatterer and is detected at any arbitrary distance z from the source as represented in Fig. 4.1. The complex field at the detector plane is represented as

$$E(r) = FR\left[E(\hat{r})\,\mathrm{e}^{i\delta(\hat{r})}\right] = E_x(r)\hat{e}_x + E_y(r)\hat{e}_y, \tag{4.2}$$

where $E(r)$ indicates the random field at the detector plane. FR is Fresnel transform to accommodate the propagation effect from the scattering plane to the detector plane located at distance z. $\delta(\hat{r})$ indicates the stochastic phase introduced by the diffuser, r is the transverse spatial position vector at the detector plane. The random field at the detector plane, situated in the Fresnel regime, and given as

$$E(r) = \int G(r,\hat{r})E(\hat{r})e^{i\delta(\hat{r})}d\hat{r}, \tag{4.3}$$

For the free space propagation, the Fresnel Kernel is represented as

$$G(r,\hat{r}) = \frac{\exp(ikz)}{i\lambda z}\exp\left(ik\frac{|\hat{r}|^2 + |r|^2 - 2r.\hat{r}}{2z}\right). \tag{4.4}$$

All symbols have their usual meaning. The SPs of the instantaneous random field are expressed as

$$S_p(r) = \sum_{a,b}\sigma_{ab}^{p}E_a^{*}(r)E_b(r),\ (a, b=x, y\ \&\ p=0, 1, 2, 3) \tag{4.5}$$

where the 2x2 identity matrix σ^0 and the three Pauli spin matrices.

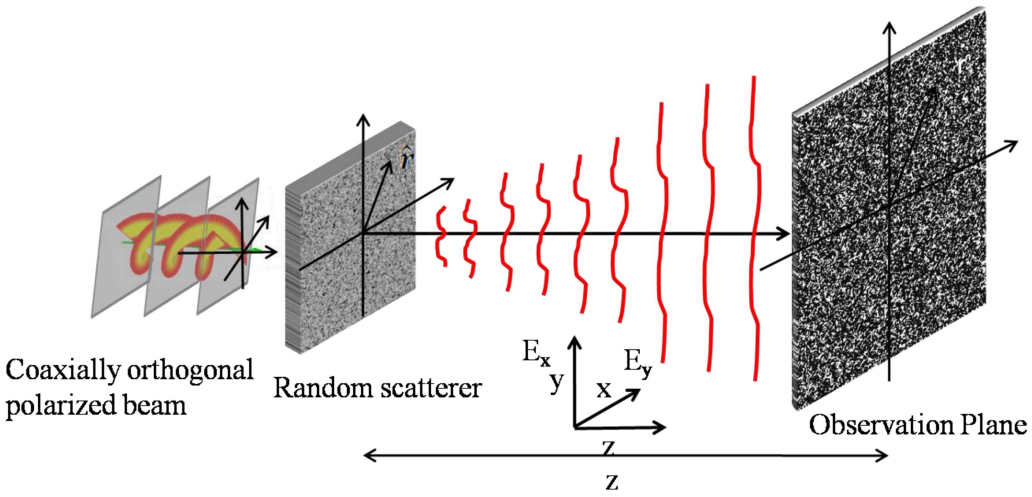

Fig. 4.1 Schematic representation of the creation of the random electromagnetic field by orthogonally polarized incident light fields.

The SPs fluctuations with respect to their average value are expressed as

$$\Delta S_p(r) = S_p(r) - < S_p(r) >, \tag{4.6}$$

where $S_p(r)$ is the SP at a special spatial point and $<S_p(r)>$ indicates the average value. The statistical features of the random light are characterized by correlations between the SPs fluctuations. All presumable pairs of the two-point SPs correlation are described by a 4x4 matrix $C_{pq}(r_1, r_2)$ with elements (Kuebel, 2019)

$$\begin{aligned} C_{pq}(r_1, r_2) &= \left\langle \Delta S_p(r_1) \Delta S_q(r_2) \right\rangle \\ &= \left\langle S_p(r_1) S_q(r_2) \right\rangle - \left\langle S_p(r_1) \right\rangle \left\langle S_q(r_2) \right\rangle \\ &= \sum_{a,b} \sum_{c,d} \sigma_{ab}^{p} \sigma_{cd}^{q} \left\langle E_a^*(r_1) E_b(r_1) E_c^*(r_2) E_d(r_2) \right\rangle \\ &\quad - \sum_{a,b} \sigma_{ab}^{n} \left\langle E_a^*(r_1) E_b(r_1) \right\rangle \sum_{c,d} \sigma_{cd}^{m} \left\langle E_c^*(r_2) E_d(r_2) \right\rangle . \end{aligned} \tag{4.7}$$

where r_1 and r_2 are two transverse spatial coordinates at the detector plane and parenthesis $\langle . \rangle$ indicates the ensemble average. Now Gaussian moment theorem is applied to convert the 4th-order correlation into a 2nd-order correlation. Therefore the correlation matrix $C_{pq}(r_1, r_2)$ is represented as

$$C_{pq}(r_1, r_2) = \sum_{a,b}\sum_{c,d} \sigma_{ab}^{p} \sigma_{cd}^{q} \left[\left\langle E_a^*(r_1) E_b(r_1) \right\rangle \left\langle E_c^*(r_2) E_d(r_2) \right\rangle + \left\langle E_a^*(r_1) E_d(r_2) \right\rangle \left\langle E_c^*(r_2) E_b(r_1) \right\rangle \right]$$

$$- \sum_{a,b}\sum_{c,d} \sigma_{ab}^{p} \sigma_{cd}^{q} \left\langle E_a^*(r_1) E_b(r_1) \right\rangle \left\langle E_c^*(r_2) E_d(r_2) \right\rangle$$

$$= \sum_{a,b}\sum_{c,d} \sigma_{ab}^{p} \sigma_{cd}^{q} W_{ad}(r_1, r_2) W_{bc}^*(r_1, r_2). \tag{4.8}$$

where $W_{ad}(r_1, r_2) = \langle E_a^*(r_1) E_d(r_2) \rangle$ are the elements of the 2x2 coherence-polarization (CP) matrix which characterizes the vectorial stochastic field (Wolf, 2007)

$$W(r_1, r_2) = \begin{pmatrix} W_{xx}(r_1, r_2) & W_{xy}(r_1, r_2) \\ W_{yx}(r_1, r_2) & W_{yy}(r_1, r_2) \end{pmatrix} \tag{4.9}$$

Therefore, all pairs of SPs fluctuations correlation are represented as

$$C_{pq}(r_1, r_2) = \begin{pmatrix} C_{00}(r_1, r_2) & C_{01}(r_1, r_2) & C_{02}(r_1, r_2) & C_{03}(r_1, r_2) \\ C_{10}(r_1, r_2) & C_{11}(r_1, r_2) & C_{12}(r_1, r_2) & C_{13}(r_1, r_2) \\ C_{20}(r_1, r_2) & C_{21}(r_1, r_2) & C_{22}(r_1, r_2) & C_{23}(r_1, r_2) \\ C_{30}(r_1, r_2) & C_{31}(r_1, r_2) & C_{32}(r_1, r_2) & C_{33}(r_1, r_2) \end{pmatrix}, \tag{4.10}$$

The element $C_{23}(r_1, r_2)$ of the matrix is evaluated using Eq. (4.8)

$$C_{23}(r_1, r_2) = \sum_{a,b}\sum_{c,d} \sigma_{ab}^{2} \sigma_{cd}^{3} W_{ad}(r_1, r_2) W_{bc}^*(r_1, r_2).$$

$$\propto \mathrm{Im}[W_{xy}(r_1, r_2) W_{yx}^*(r_1, r_2) + W_{xx}^*(r_1, r_2) W_{yy}(r_1, r_2)].$$

$$\propto \mathrm{Im}[A+B]. \tag{4.11}$$

where $A = W_{xy}(r_1, r_2)W^*_{yx}(r_1, r_2)$, and $B = W^*_{xx}(r_1, r_2)W_{yy}(r_1, r_2)$.

Let us explore the use of Eq. (4.11) in the estimation of the TC from the speckle pattern.

$$A = W_{xy}(r_1, r_2)W^*_{yx}(r_1, r_2) = \left\langle E^*_x(r_1)E_y(r_2)\right\rangle\left\langle [E^*_y(r_1)E_x(r_2)]^*\right\rangle, \tag{4.12}$$

Substituting Eq. (4.3) into the SPs correlation results in the cancellation of the phase term outside the Fresnel propagation kernel as shown in Eq. (4.3) and hence this phase term is ignored in Eq. (4.12) (Singh, R., 2017). The SPs correlation helps to achieve spatial stationarity at any arbitrary z and this allows the replacement of the ensemble averaging by spatial averaging as discussed in chapter 1.

$$W_{ab}(\Delta r) \propto \int E^*_a(\hat{r})E_b(\hat{r})\exp\left(-\frac{ik\Delta r.\hat{r}}{z}\right)d\hat{r}, \qquad (a,\ b{=}x,\ y) \tag{4.13}$$

Here, we consider $E_x(\hat{r}) = \exp(il\varphi)$ is embedded in a circular aperture $cir\left(\frac{\hat{r}}{a}\right)$ where a is the radius and $U_y(\hat{r}) = 1$. Therefore Eq. (4.13) transforms to

$$W_{xy}(\Delta r) \propto \frac{J_1(2\pi a\Delta r/\lambda z)}{2\pi a\Delta r/\lambda z}\exp(-im\Delta\varphi), \tag{4.14}$$

where J_1 represents the Bessel function. Similarly, $W^*_{yx}(\Delta r) \propto \frac{J_1(2\pi a\Delta r/\lambda z)}{2\pi a\Delta r/\lambda z}\exp(-il\Delta\varphi)$,

$W^*_{xx}(\Delta r) \propto \frac{J_1(2\pi a\Delta r/\lambda z)}{2\pi a\Delta r/\lambda z}$, and $W_{yy}(\Delta r) \propto 1$.

Substituting the value of $W_{xy}(\Delta r), W^*_{yx}(\Delta r), W^*_{xx}(\Delta r)$, and $W_{yy}(\Delta r)$, into Eq. (4.11). Therefore Eq. (4.11) modifies it as

$$C_{23}(\Delta r) \propto \mathrm{Im}\left[\left(\frac{J_1(2\pi a\Delta r/\lambda z)}{2\pi a\Delta r/\lambda z}\exp(-il\Delta\varphi)\right)^2 + \frac{J_1(2\pi a\Delta r/\lambda z)}{2\pi a\Delta r/\lambda z}\right], \tag{4.15}$$

Eq. (4.15) connects the source and Stokes correlation function at the detector plane and the distribution of cross-covariance helps to make a relation between topological charge and petals to estimate TC. The distribution of the correlation function forms petals due to the imaginary part $\mathrm{Sin}\,2(\Delta\varphi)$ of the cross-covariance function $C_{23}(\Delta r)$.

This empirical relation is represented as

$$n = 4l, \qquad (m,\ n=0,\ 1,\ 2,\ 3,\ldots\ldots) \tag{4.16}$$

where *l* represents the topological charge and *n* denotes petals.

4.3 Simulation results

To illustrate the validation of our approach, we simulated an experimental situation wherein an orthogonally polarized beam i.e x-polarized beam is encoded with the helical phase and a y-polarized beam is a plane wave, and both are coaxially propagating through the random scattering media as represented in Fig. 1 (b). We have simulated the different vortex beams with TC *l*=1, 2, 3. Simulation is realized for orthogonally polarized random light fields with wavelength $\lambda = 632.8$ nm. The random fields for coaxially orthogonal polarization components are modeled by considering the phase screens with phase variation with equal probability distribution in the range of $[-\pi, \pi]$. A random field coming out from the scattering media propagates from the source to the observation plane at z=250 mm. The Stokes parameters of the random field at the observation plane are obtained from the digitally propagated coherent random fields.

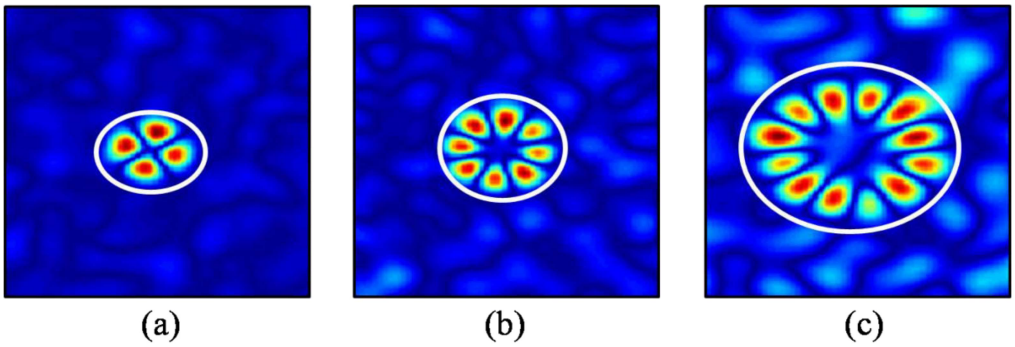

Fig. 4.2 (a-c) Represent simulation results for the distribution of correlation function for vortex with *m=1, 2, 3* respectively.

These simulated Stokes parameters are used to extract the higher-order Stokes fluctuations correlations as explained in Eq. (4.15) and utilized to estimate the TC of the vortex beam. The higher-order Stokes fluctuation correlation $C_{23}(\Delta r)$ is obtained by using spatial averaging as follows. The spatial averaging is executed by selecting 1000 x 1000 pixels of random patterns from the captured SPs (S_2, S_3), and 2D scanning of $S_n^{\alpha}(x, y)$ where x, y are the pixel spatial coordinates and takes value up to 300 x 300 provides 700 x 700 random patterns for averaging. Simulation results of the distribution of cross-covariance are represented in Fig. 4.2. Simulation results in Fig. 4.2, (a)-(c) represent a distribution of polarization correlation function $C_{23}(\Delta r)$ for vortex with *l=1, 2, 3*respectively. The distribution of coherence function forms 4, 8, and 12 petals for vortex with *l=1, l=2,* and *l=3* are represented in Figs. 4.2, (a-c) respectively.

4.4 Experiment

To experimentally demonstrate the proposed method in a lensless configuration, we designed an experimental set-up as shown in Fig. 4.3. Detailed description of the experimental method is as follows. A spatially filtered collimated He-Ne laser light beam is attenuated with a neutral density filter (NDF) and oriented at 45°with respect to the horizontal direction using a half-wave plate (HWP). The 45° polarized beam splits into

two equal-intensity beams by the beam splitter BS. A beam transmitted from the BS illuminates a phase-only SLM with a resolution of 1920 x 1080 and a pixel pitch of 8 μm (Pluto from Holoeye) on which the structure of the helical phase is displayed. Consequently, the structure of the helical information is loaded into the x-polarization component of the beam and the y-polarization component remains intact, i.e. no vortex. The beam coming from the SLM reflects by the BS and travels through the ground glass and random scattering from the ground glass (GG) distorts the incident light and generates a speckle pattern. In order to detect the polarization states of the randomly scattered light, we use optical elements to measure the SPs.

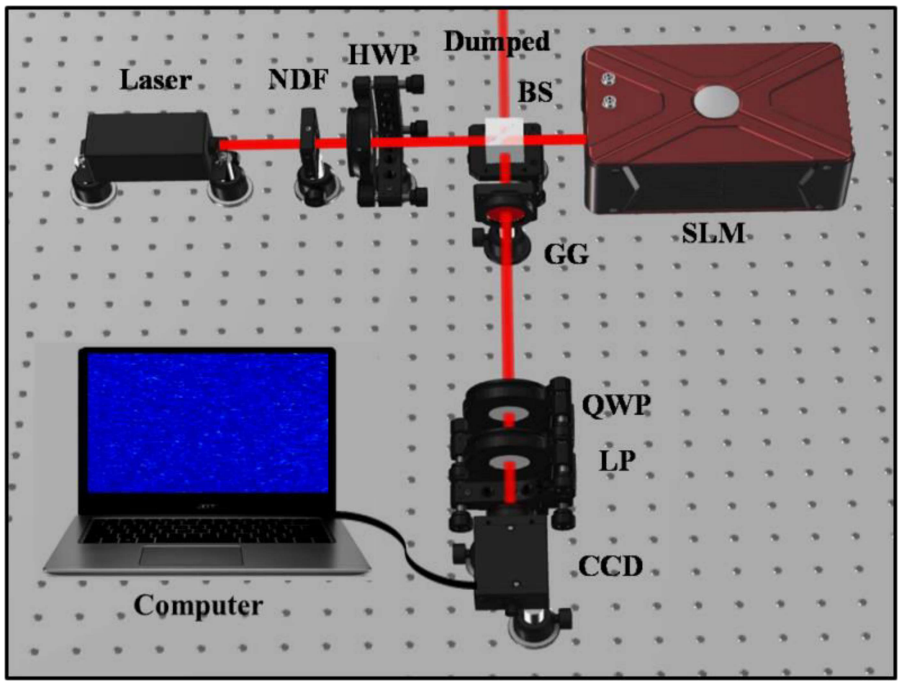

Fig. 4.3 An experimental setup to estimate the TC of the vortex beam from the speckle pattern. NDF: neutral density filter, HWP: half-wave plate, BS: beam splitter, SLM: spatial light modulator, GG: ground glass, QWP: quarter-wave plate, LP: linear polarizer, CCD: charge-coupled device. The dumped beam is not used in the experiment.

The random light further passes through a QWP, which is rotated at an angle θ_q with respect to the x-direction and filtered by an LP. The transmission axis of the LP is placed

in the x-direction with respect to the QWP and the resultant field is captured by a CCD camera with a dynamic range of 8-bit and resolution of 1280 x 1024 pixels and a pixel pitch of 4.65 micron [Thorlab model No. DCU224M] which was placed at a distance z= 250 mm from the diffuser. The intensity speckle patterns are recorded by the CCD camera. The four SPs are determined from the recorded speckle patterns by using the following equations (Goldstein, 2017).

$$S_2(r) = I(45^o, 45^o) - I(135^o, 135^o),$$
$$S_3(r) = I(0^o, 45^o) - I(0^o, 135^o), \tag{4.17}$$

where $I(\theta_q, \theta_p)$ is the intensity at the observation plane. θ_q is the orientation of the optic axis of the quarter-wave plate with the axis of the polarizer and θ_p is the angle of the polarizer with the x-axis. The experimentally measured SPs are used to evaluate the correlation between SPs fluctuation using Eq. (4.7) and ensemble averaging is replaced by spatial averaging. This process is applied to evaluate cross-covariance $C_{23}(\Delta r)$ from the experimentally detected SPs as described in Eq. (4.15). Finally, the topological charge is estimated by counting petals as described in Eq. (4.16).

4.5 Results and discussions

The SPs are measured from the experimentally captured intensity speckle pattern for the helical beams with *l=1, 2, 3,* and the results are represented in Fig. 4.4. Fig. 4.4, (a), (b) denote recorded SPs (S_2, S_3) from the random intensity pattern for vortex with *l=1*.

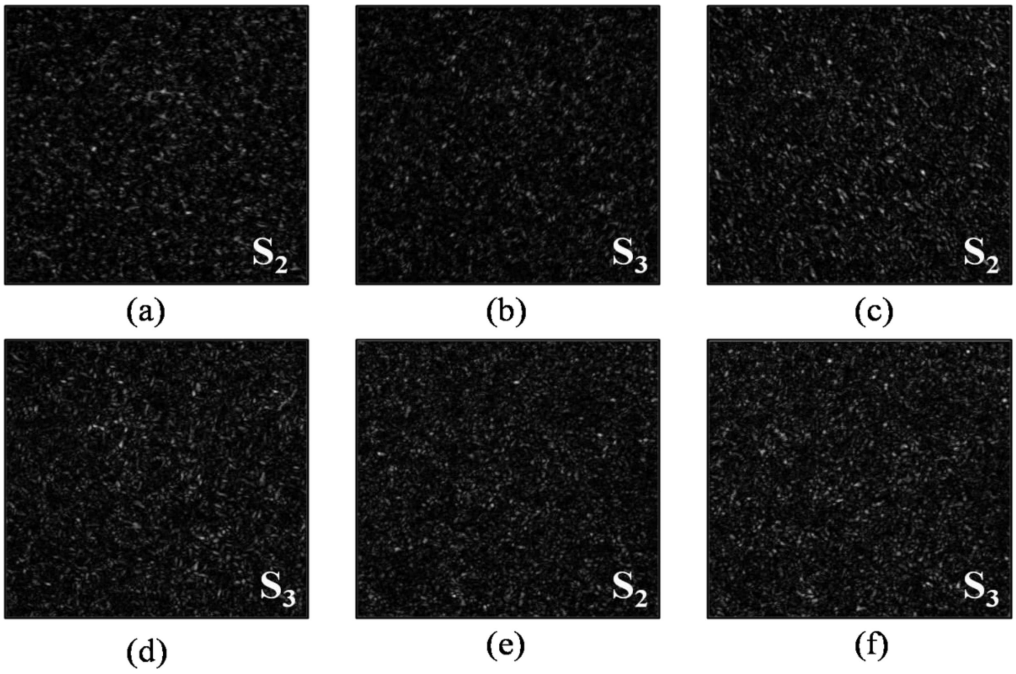

Fig. 4.4 Denotes experimentally measured SPs from the recorded intensity speckle patterns. **(a, b)**, **(c, d)**, **(e, f)** show SPs of the vortex with *l=1, 2, 3* respectively.

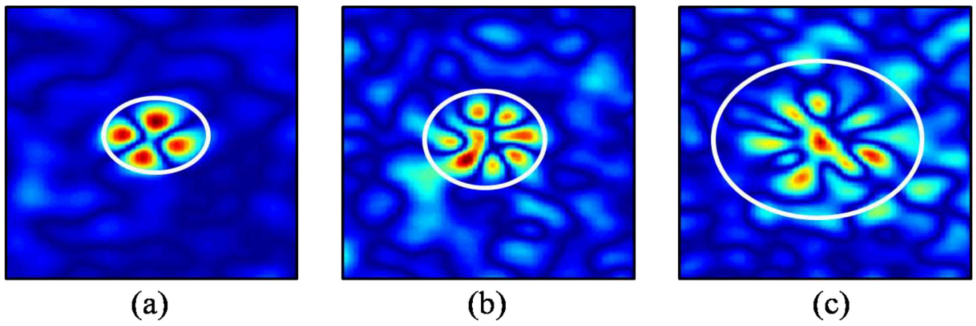

Fig. 4.5 (a-c) Represent experimental results for the distribution of correlation function for vortex with *m=1, 2, 3* respectively.

Fig. 4.4, (c), (d) show SPs (S_2, S_3) for vortex with *l=2* and Fig. 4.4, (e), (f) denote SPs (S_2, S_3) for vortex with *l=3* respectively. Experimental results of the distribution of cross-covariance are represented in Fig. 4.5. Experimental results in Fig. 4.5, (a-c) represent a distribution of polarization correlation function $C_{23}(\Delta r)$ for vortex with *l=1, 2, 3* respectively. The distribution of correlation function forms 4, 8, and 12 petals for vortex

with *l=1,l=2,* and *l=3* are represented in Figs. 4.5, (a), (b), and (c) respectively. A small deviation in the experimental results in comparison to the simulation is possibly owing to experimental constraints. Some weak residual modes for corresponding field distribution may appear due to the phase profile used to generate vortex using pixilated SLM. On the other hand, limited size polarization optics in the experiment and background coherence $W_{xx}^{*}(\Delta r),$ and $W_{yy}(\Delta r)$ in Eq. (4.13) also affects the reconstruction quality.

4.6 Conclusion

In this chapter, we have proposed and experimentally demonstrated a new approach to estimating the TC of the helical beam propagating through the random scattering medium. The SPs of the random light are utilized to evaluate the higher-order SPs fluctuation correlation and subsequently applied for the efficient estimation of the incident helical beam. The distribution of the cross-covariance renders the information of the TC of the helical beam. The feasibility of the proposed approach is evaluated by numerical simulation and followed by the experimental demonstration for the estimation of TC of the helical beam. The proposed experimental configuration is robust and offers flexibility owing to non-interferometric. The applicability of the developed approach has been experimentally demonstrated to estimate helical beams with *m=1, 2, 3.*